Supplemental information: Kinetics of Shear Banding Flow Formation in Linear and Branched Wormlike Micelles

Peter Rassolov, Alfredo Scigliani, and Hadi Mohammadigoushki*
Department of Chemical and Biomedical Engineering,
FAMU-FSU College of Engineering, Tallahassee, FL, 32310, USA

(Dated: July 28, 2022)

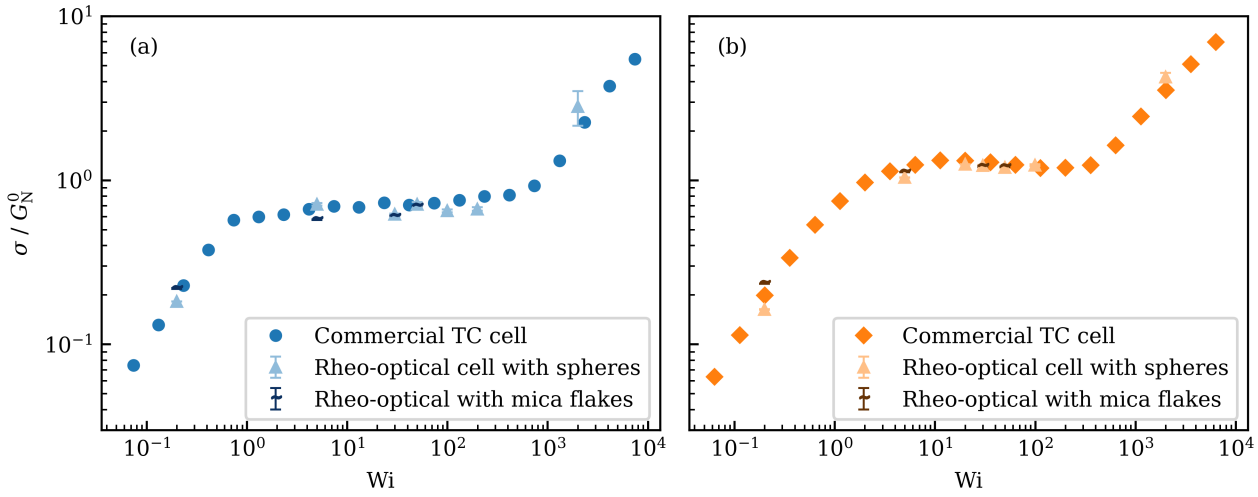

FIG. S1. Flow curves for linear (a) and branched (b) WLM solutions obtained via commercial TC cell and the Rheo-optical cell confirming that they are not changed by the addition of mica flakes or seeding particles.

I. FITTING FUNCTION FOR ESTIMATION OF THE SHEAR RATE INHOMOGENEITY PARAMETER

As discussed in the main text, computing the local shear rate accurately from an experimentally obtained velocity profile by purely numerical means is challenging. However, if the velocity data follows a known analytical expression, one can instead fit the expression to the data, then compute the necessary derivative(s) analytically. For two-shear-band profiles, whether transient or quasi-steady, a suitable expression for the shear rate is a sigmoidal function:

$$\dot{\gamma}(x) = \dot{\gamma}_l + \frac{\dot{\gamma}_h - \dot{\gamma}_l}{1 + \exp\left[(x - x_i)/w\right]}, \tag{S1}$$

where $\dot{\gamma}_h$ and $\dot{\gamma}_l$ are the local shear rates in the high and low shear rate bands, x_i is the location of the interface between the high and low shear bands, and w is a parameter representing

* Corresponding Author: hadi.moham@eng.famu.fsu.edu

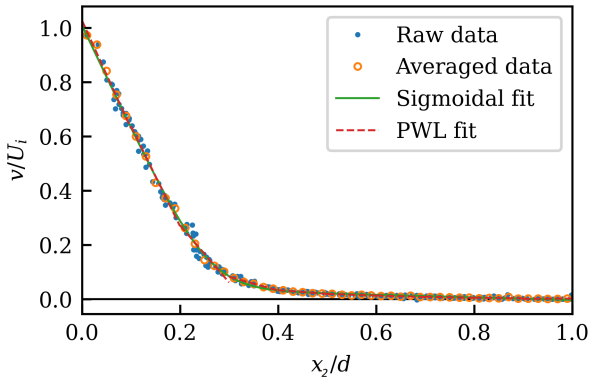

FIG. S2. Example plot showing fitting methods for quantifying Δ. Shown are rheo-PTV raw data obtained for linear WLMs at Wi = 50 and $\gamma = 136$ (blue dots), space-time element averages (empty orange circles), sigmoidal shear banding velocity profile fitted to the raw data (continuous green line), and velocity profile estimated from piecewise linear fitting to the raw data (dashed red lines).

the interface width. If the curvature is small enough that the flow field can be approximated as rectilinear with $\dot{\gamma} = -dv/dx$, the local velocity profile v can be computed analytically as follows:

$$v(x) = \mathcal{C} - \dot{\gamma}_l x + (\dot{\gamma}_h - \dot{\gamma}_l)\left\{w \log\left[1 + \exp\left(\frac{x - x_i}{w}\right)\right] - (x - x_i)\right\}, \tag{S2}$$

where $\mathcal{C}$ is the constant of integration and can either serve as an additional fitting parameter to allow for wall slip or be defined such that $v(x = 0) = v_i$. Following the determination of parameters by fitting Equation S2 to the experimental data, computing the shear rate inhomogeneity parameter Δ is straightforward. There are no local maxima or minima in Equation S1; therefore, $\dot{\gamma}_{max}$ and $\dot{\gamma}_{min}$ can be replaced with the local shear rates at the inner and outer cylinders:

$$\Delta = \frac{|\dot{\gamma}(x_2 = 0) - \dot{\gamma}(x_2 = d)|}{v_i/d} \tag{S3}$$

In cases where there is wall slip, the denominator in Equation S3 is modified by replacing v_i with $v(x_2 = 0) - v(x_2 = d)$; however, no wall slip was observed in this study.

For a Newtonian fluid, the shear rate in the cylindrical Couette geometry can be analytically obtained from the Navier-Stokes equation as follows:

$$\dot{\gamma}(r) = \left| r\frac{\partial}{\partial r}\left(\frac{v}{r}\right)\right| = \frac{2R_i {R_o}^2}{{R_o}^2 - {R_i}^2}\frac{v_i}{r}, \tag{S4}$$

where $r = x_2 + R_i$. Consequently, the shear rate inhomogeneity parameter for the Newtonian fluid is a constant $\Delta_N = \frac{2d}{R_i} = 0.176$.

II. ADDITIONAL RHEOLOGICAL PROPERTIES OF THE WORMLIKE MICELLAR SOLUTIONS

In addition to the flow curves and the Cole-Cole plots reported in the main body of the manuscript, in Fig. S3(a), we show the viscosity of the micellar solutions measured as a function of shear rate along with the best fit to the Carreau-Yasuda model (solid curves). The Carreau-Yasuda model expression is $\eta(\dot{\gamma}) = (\eta_0 - \eta_\infty)\,[1 + (\lambda_c\dot{\gamma})^a]^{(n-1)/a} + \eta_\infty$ [K. Yasuda, et al., *Rheol. Acta*, 1981, **20**, 163.], and the model parameters are listed in Table. S1 below. In addition, Fig. S3 (b) shows the SAOS results in terms of the storage and loss moduli as a function of angular frequency for both linear and branched micellar solutions.

In addition, the elasticity number E is calculated for both solutions as $E = Wi/Re = \eta_0\lambda/\rho d^2$ and the data are shown for both linear and branched micellar solutions in Table S1. Note that the relaxation times of these fluids are obtained by fitting a single-mode Maxwell model to the SAOS data.

Micellar system	η_0 [Pa.s]	η_∞ [Pa.s]	λ_c [s]	a	n	λ [s]	G^0_N [Pa]	E
Linear	36.3	2.3×10^{-2}	113	2.92	0.0	74.0	0.5	1.93×10^6
Branched	36.8	3.6×10^{-2}	54	1.78	0.0	63.6	0.57	1.69×10^6

TABLE S1. Carreau-Yasuda model parameters, relaxation time, and elasticity number for the selected linear and branched WLM solutions.

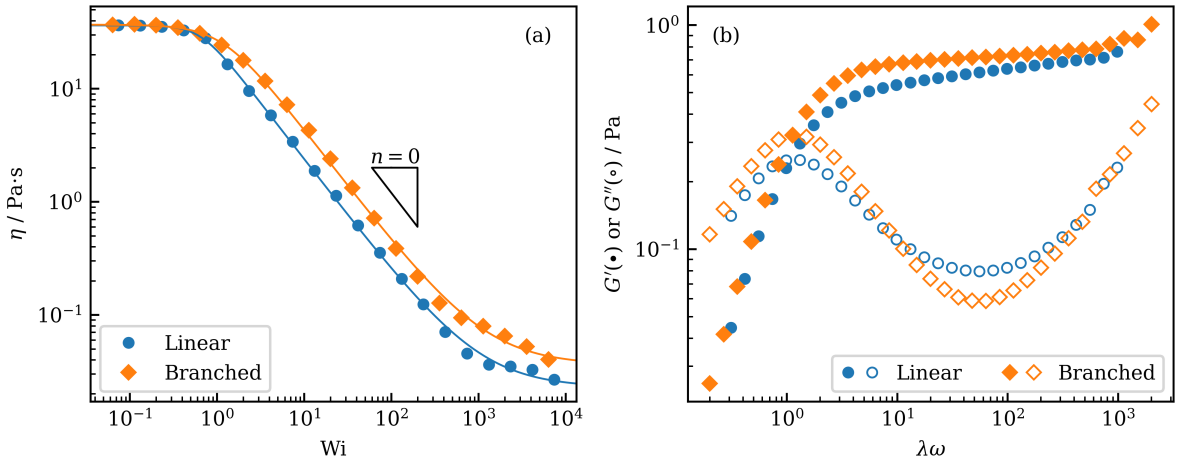

FIG. S3. (a) Viscosity as a function of Wi for the selected linear and branched WLM solutions showing that there is a shear stress plateau with power law index equal to zero for both. The solid curves are the best fits of the Carreau-Yasuda model to the experimental data with parameters given in Table S1. (b) Storage (filled symbols) and loss (empty symbols) moduli as a function of dimensionless angular frequency for the selected linear and branched WLM solutions.

III. ADDITIONAL FIGURES

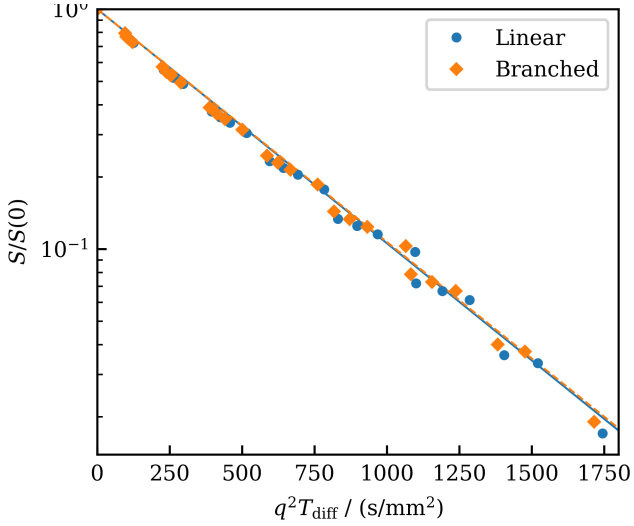

FIG. S4. Normalized NMR signal intensity of the water peak as a function of diffusion weighting in linear and branched WLMs. Lines are best fits to a mono-exponential decay for α =1. The mean square displacement $Z = 2DT_{diff}$, where D is the apparent diffusion coefficient. Based on this fitting the diffusion coefficient of water $D = 2.2 \times 10^{-9}$ m^2/s both for linear and branched WLMs. This value is close to reported diffusion coefficient of water $D \approx 2.1 \times 10^{-9}$ m^2/s at $T = 21°$C [1, 2].

[1] M. Holz, S. R. Heil and A. Sacco, Phys. Chem. Chem. Phys., 2000, **2**, 4740–4742.
[2] P. Tofts, D. Lloyd, C. Clark, G. Barker, G. Parker, P. McConville, C. Baldock and J. Pope, Magnetic Resonance in Medicine: An Official Journal of the International Society for Magnetic Resonance in Medicine, 2000, **43**, 368–374.

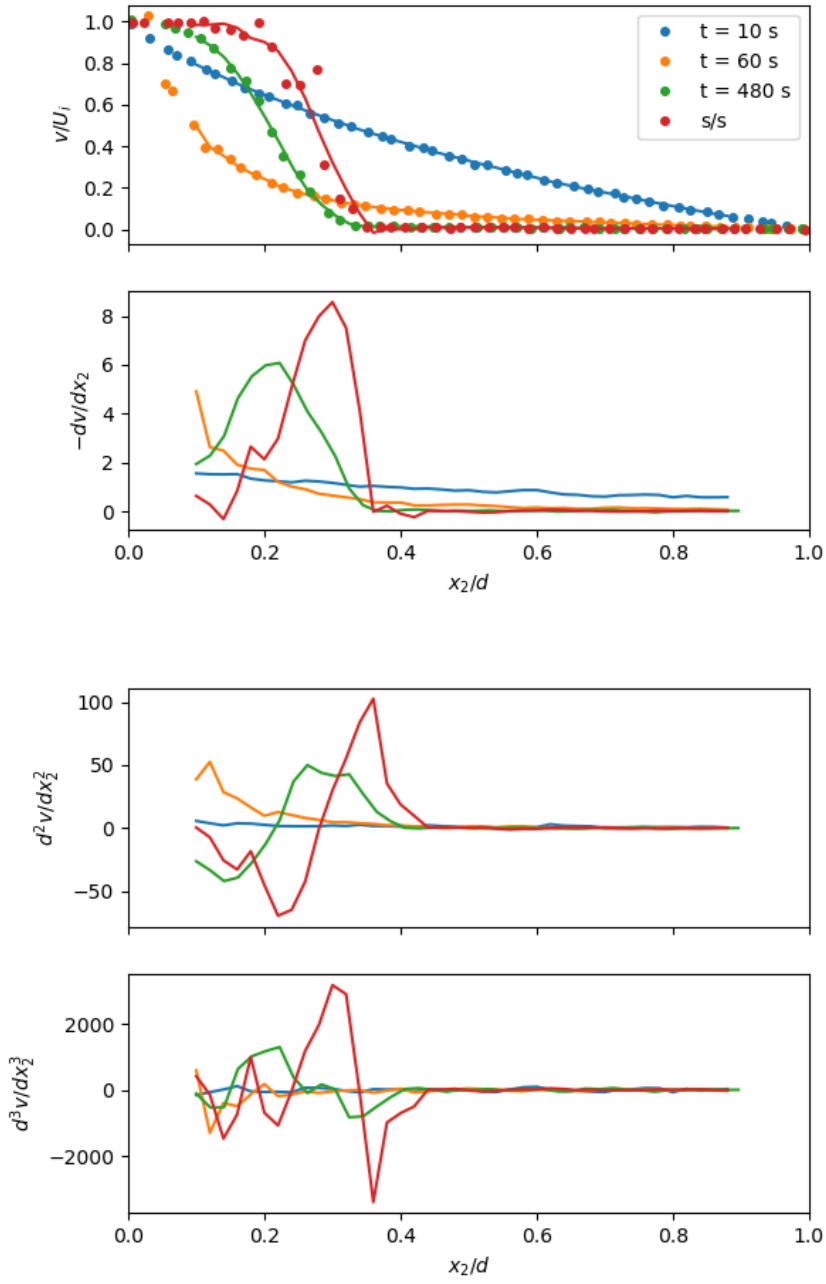

FIG. S5. Selected velocity profiles for linear WLMs with first, second, and third order derivatives estimated by local third-order polynomial fitting. The smoothing parameter p is 0.2.

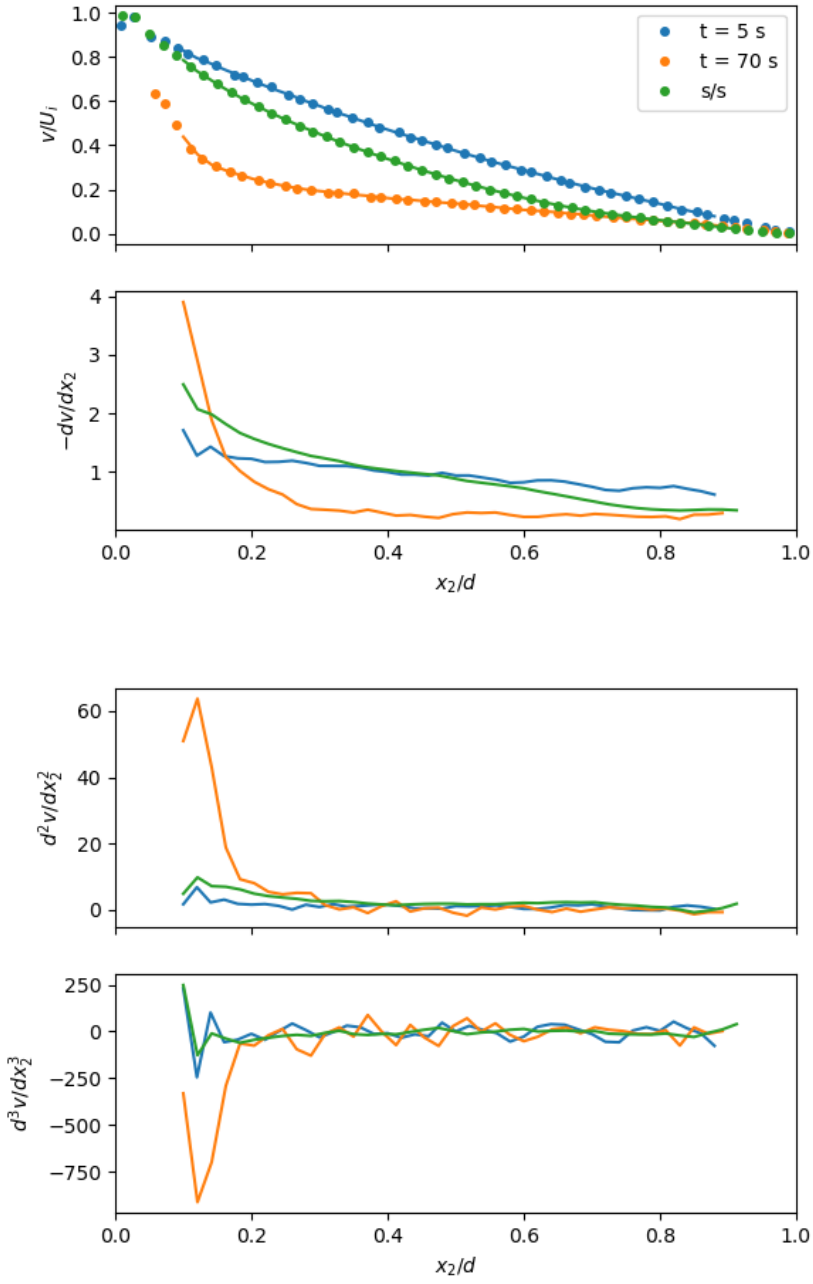

FIG. S6. Selected velocity profiles for branched WLMs with first, second, and third order derivatives estimated by local low-order polynomial fitting. The smoothing parameter p is 0.2.

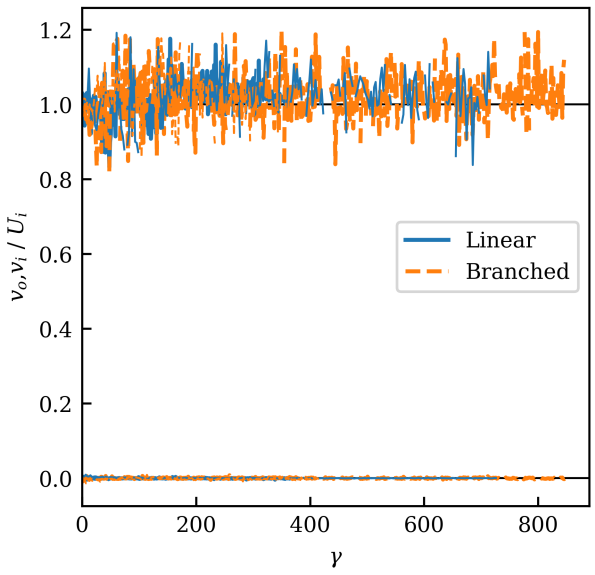

FIG. S7. Evolution of wall slip for Wi = 50 (broad lines) and 200 (narrow lines) for linear and branched WLM solutions. Fluid velocities at the inner ($v/U_i \approx 1$) and outer ($v \approx 0$) cylinders estimated from piecewise linear fitting are plotted; horizontal lines indicate the velocity of each wall.

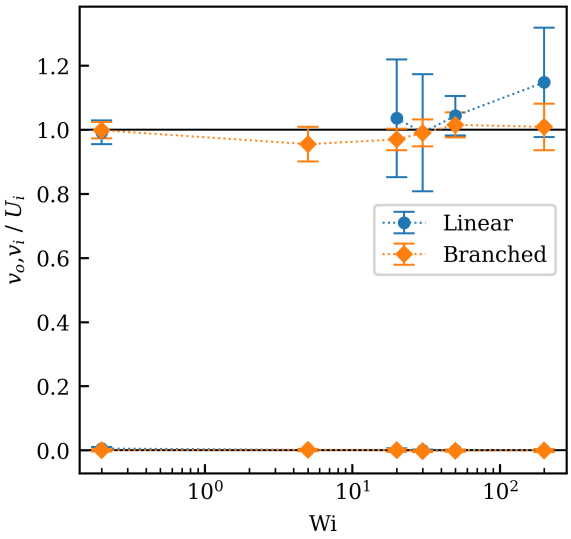

FIG. S8. Quasi-steady fluid velocity at each wall estimated from piecewise linear fitting for linear and branched WLM solutions at the inner ($v \approx 1$) and outer ($v \approx 0$) cylinders. For linear WLMs at Wi = 5, the high shear rate band is very narrow (see Fig. S9) and cannot be accurately extrapolated to the wall.

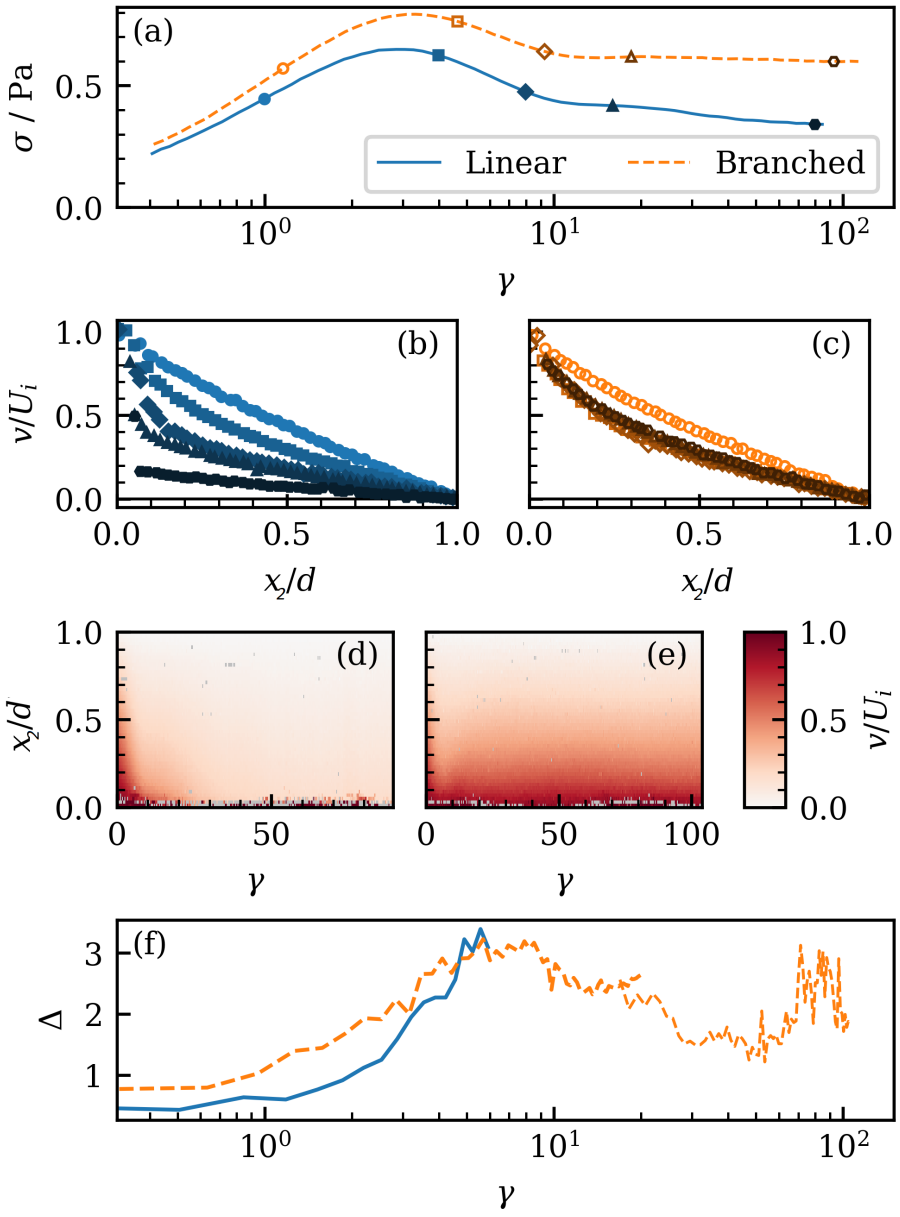

FIG. S9. Local velocimetry of linear and branched WLMs at applied Wi = 5: (a) shear stress evolution with shear strain, (b,c) selected velocity profiles for (b) linear and (c) branched WLMs, (d,e) maps of local velocity evolution with shear strain, (f) evolution of the shear rate inhomogeneity parameter Δ with shear strain. In subfigure (f), Δ values are not reported in linear wormlike micelles for $\gamma > 6$. This is because the width of the high shear band is thin and cannot be resolved in experiments, which in turn makes the accurate estimation of Δ difficult.

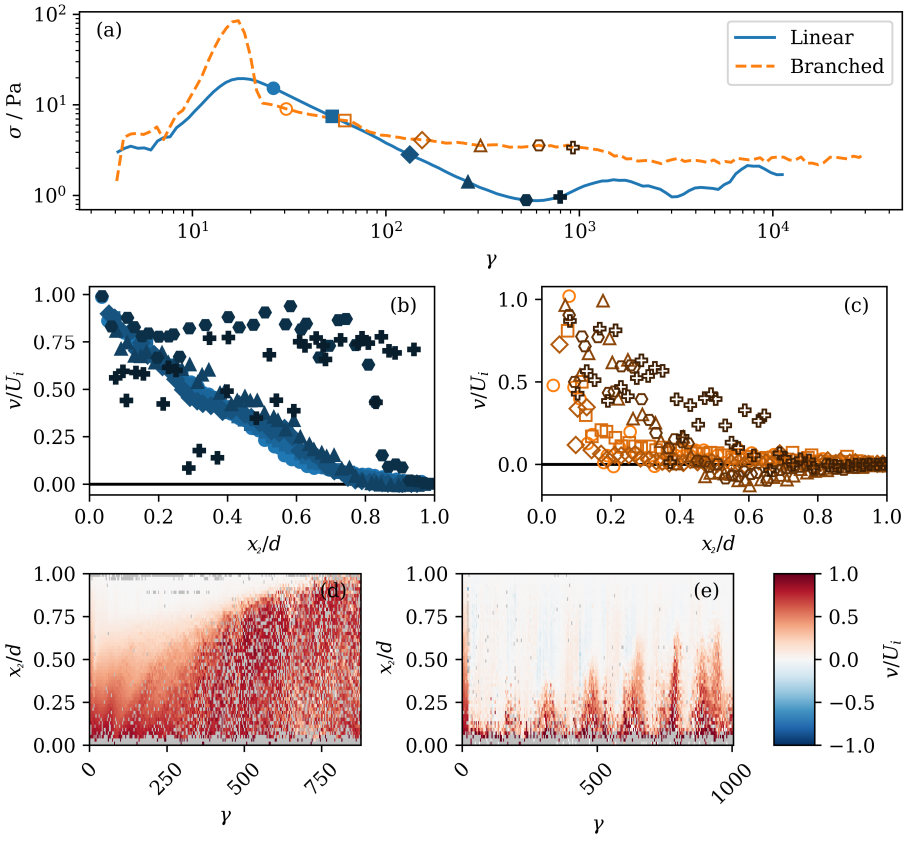

FIG. S10. Local velocimetry of linear and branched WLMs at applied Wi = 2000: (a) shear stress evolution with shear strain, (b,c) selected velocity profiles for (b) linear and (c) branched WLMs, (d,e) maps of local velocity evolution with shear strain.

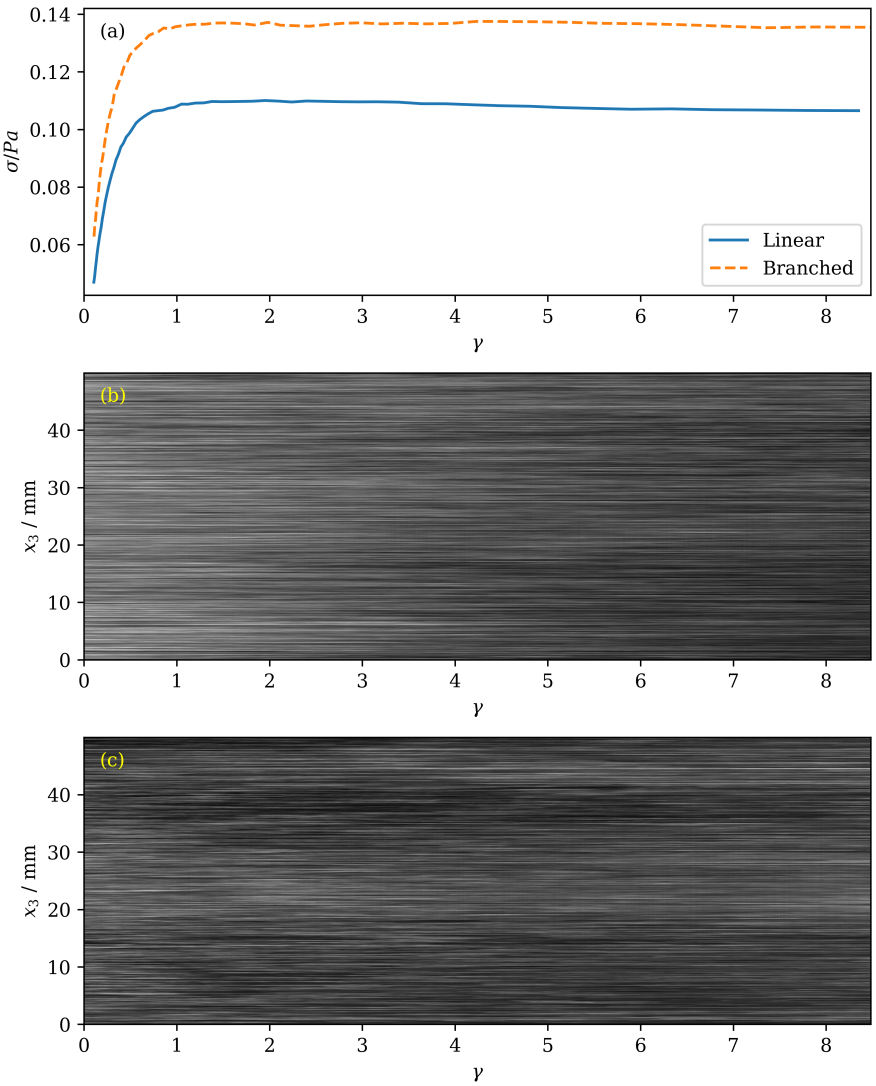

FIG. S11. Flow stability visualized with mica flakes for linear and branched WLMs at Wi = 0.2. (a) Shear stress evolution with shear strain. (b) Visualized flow with increasing shear strain for linear WLMs. (c) Visualized flow with increasing shear strain for branched WLMs.

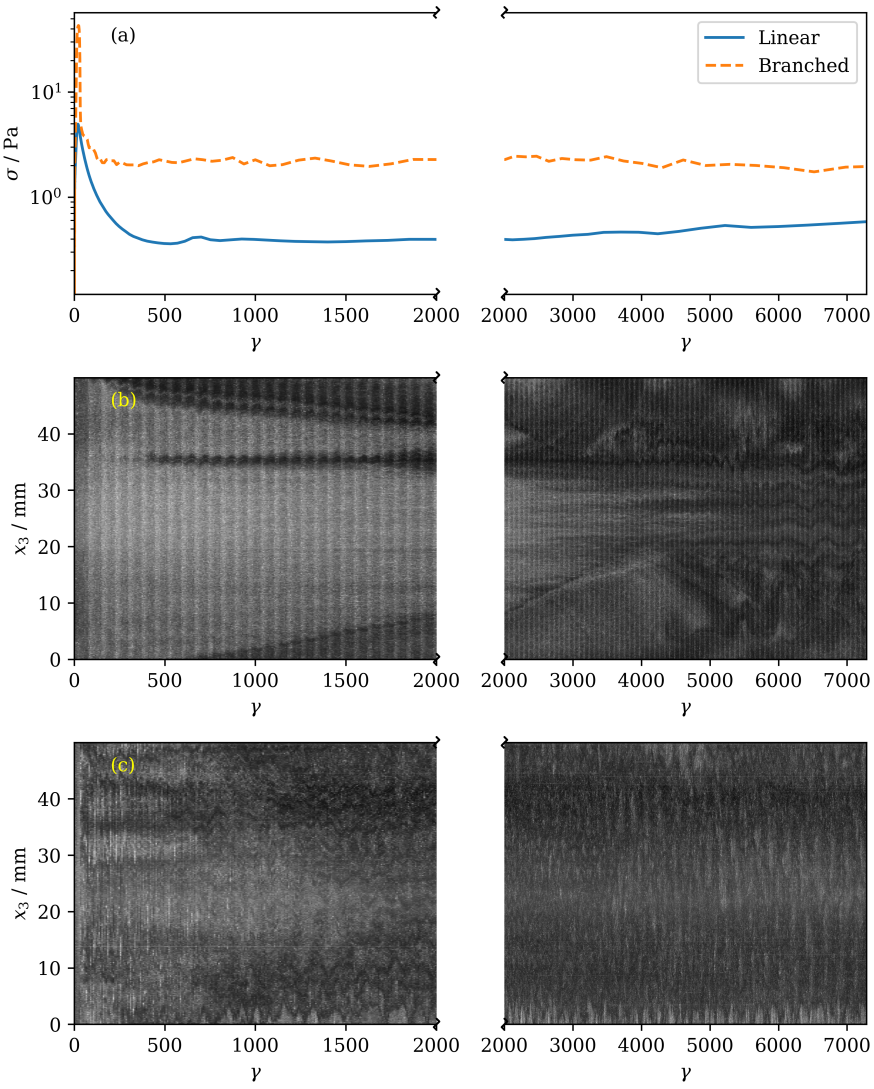

FIG. S12. Flow instabilities visualized with mica flakes for linear and branched WLMs at Wi = 500. (a) Shear stress evolution with shear strain. (b) Visualized flow with increasing shear strain for linear WLMs. (c) Visualized flow with increasing shear strain for branched WLMs.

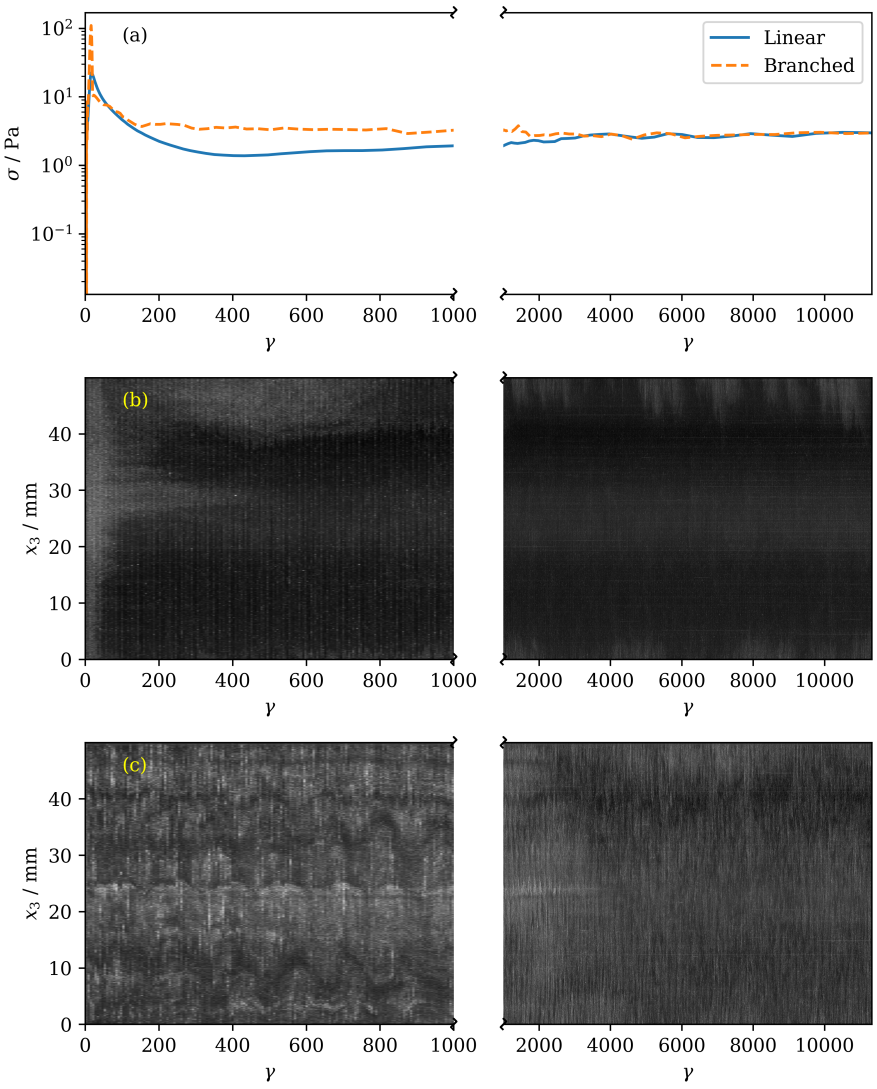

FIG. S13. Flow instabilities visualized with mica flakes for linear and branched WLMs at Wi = 2000. (a) Shear stress evolution with shear strain. (b) Visualized flow with increasing shear strain for linear WLMs. (c) Visualized flow with increasing shear strain for branched WLMs.